Plasma Dynamics with Second and Third Harmonic ECRH on TCV Tokamak

L. Porte, S. Coda, S. Alberti, G. Arnoux[(a)], P. Blanchard, A. Bortolon, A. Fasoli, T.P. Goodman, I. Klimanov, Y. Martin, M. Maslov, A. Scarabosio, H. Weisen

Ecole Polytechnique Fédérale de Lausanne (EPFL), Centre de Recherches en Physique des Plasmas, CRPP EPFL, Association EURATOM - Confédération Suisse, 1015 Lausanne, Switzerland
[(a)]Départment de Recherches sur la Fusion Contrôlée, Association EURATOM-CEA, CEA/Cadarache, 13108 Saint Paul-lez-Durance Cédex, France

email contact of main author: laurie.porte@epfl.ch

Abstract. Intense electron cyclotron resonance heating (ECRH) is employed on the TCV tokamak both in second- and third-harmonic X-mode (X2 and X3). The plasma behaviour under such conditions is driven largely by the electron dynamics, motivating extensive studies on TCV of the heating and relaxation phenomena governing both the thermal and suprathermal electron populations. The dynamics of suprathermal electrons is intimately tied to the physics of X2 current drive (ECCD). The absorption of X3 radiation has been found to be enhanced by the presence of these high-energy electrons, which can also be generated by the X3 wave itself. Electrons play a crucial role in high-density plasmas where indirect ion heating can be achieved through ion-electron collisions. Such plasmas can be heated by the X3 system enabling H-mode studies with strong electron heating. Experiments have been performed by applying X3 heating to an Ohmic H-mode target, resulting in an ELM-free regime. ECRH is also an optimal tool for manipulating the electron distribution function in both physical and velocity space. Fundamental studies of the energetic electron dynamics have been performed in TCV using periodic, low-duty-cycle bursts of ECRH, with negligible average power injection, and with electron-cyclotron-emission measurements coherently averaged over a long stationary period to improve the statistics. The characteristic times of the dynamical evolution, affected by rf diffusion and collisional scattering and slowing-down in velocity space as well as by cross-field transport in physical space, are clearly revealed by this technique.

1. Introduction

Intense electron cyclotron resonance heating (ECRH) is employed on the TCV tokamak both in second- and third-harmonic X-mode (X2 and X3) [1]. Studying the electron dynamics in the presence of ECRH is crucial to understanding the overall behaviour of plasma subjected to this form of heating. The dynamics of suprathermal electrons is intimately tied to the physics of X2 current drive (ECCD) [2-3]. The absorption of third-harmonic X-mode (X3) radiation can be enhanced by the presence of these high-energy electrons, which can also be generated by the X3 wave itself [4-6]. Suprathermal electrons are also found to be generated by the strong electric fields created by the magnetic reconnection events accompanying sawtooth crashes [7].

Electrons play an important role in high density plasmas where indirect ion heating can be achieved though ion-electron collisions. This aspect of electron dynamics is of fundamental importance to fusion relevant machines where a significant fraction of ion heating is expected through the $\alpha \rightarrow$ electron $\rightarrow$ ion channel. Access to higher density also enables the experimental study of electron heating in H-mode plasma where means are still being sought to mitigate the effects of core impurity accumulation and first wall erosion caused by ELMs.

These facets of plasma dynamics can be addressed on TCV using the X3 system, which allows access to plasma at density greatly exceeding the X2 cut-off, and particularly in H-mode [11]. The X3 apparatus also provides conditions for surgical distribution-function

engineering. The X3 beams are launched vertically from the top of the vessel, parallel to the resonant surface, in order to maximize first-pass absorption of the inherently weakly damped waves [5]. Consequently, there is a unique correspondence between the major radius and the resonant electron energy, for a given microwave frequency. While this unique correspondence is lost with X2, its short wavelength and excellent deposition localization nevertheless also make it an optimal tool for direct manipulation of the electron distribution function. Fully non-inductively sustained electron internal transport barriers in TCV [10] exemplify this, combining velocity-space control (current drive) with real-space control (shear reversal).

In this paper we will describe two recent sets of experiments, the first set aimed at heating H-mode plasma, using X3, and the second set to study the dynamics of the electron distribution function in the presence of X2 ECCD and X3 ECRH.

2 X3 Heating of H-mode Plasma

To achieve the multiple aims of obtaining high plasma beta, high ion temperature and to enlarge the operational space available to TCV an ohmic ELMy H-mode was selected as target for X3 heating. Its high temperature ($T_e \approx 1$keV; $T_i \approx 550$eV) and high energy confinement ($\tau_E \approx 45$msec) both help to increase the X3 absorption. The target was routinely accessible, exhibited good vertical stability and had a density close to the optimum for X3 heating (7×10^{19}m^{-3} : ≈ 25% of the Greenwald density). It was a single null diverted discharge with the ion diamagnetic drift direction away from the X-point. The plasma current was in the range 390kA ≤ I_p ≤ 420kA. B_φ = 1.45T, κ_{95} = 1.65 and the plasma triangularity, δ_{95}, = 0.36, while the inner plasma wall gap, d_{inner}, = 3cm and $q_{95} \approx 2.4$. The stored energy was (W_{dia}) 20kJ and the energy loss per ELM was $\delta W_{dia,ELM} / W_{dia} \approx 4\%$. The energy confinement time in these discharges was accurately predicted by IPB98(y,2) [9] scaling and it is with reference to this scaling that H-factors are calculated in this paper.

2.1 X3 Absorption in H-mode Plasma

Detailed experimental studies of third harmonic absorption have been performed on TCV [8]. The salient point for vertically launched X3 heating is the linear dependence of the absorption on electron temperature (T_e). It has also been shown [8] that, in H-mode plasmas, estimates of X3 power absorption, obtained using TORAY-GA [13], are in good agreement with measurements made using a diamagnetic loop [12]. All estimates of X3 absorbed power, presented in this paper, have been obtained using TORAY-GA. Typically, at the start of the X3 heating phase, when the electron temperature was ≈ 1keV, only 35% of X3 power was coupled to the plasma but it quickly increased to > 70% (1.0MW of coupled X3 power) as T_e increased from 1.0keV to 3.0keV. At the same time the ohmic power fell from 500kW to 350kW. The total heating power therefore increased from 500kW to 1.35MW. Figure 1a shows the X3 power absorption as a function of normalised radius (ρ) in a case where the electron temperature was ≈ 2.keV and the electron density was near optimal.

The power deposition volume lay in the region 0.1 ≤ ρ ≤ 0.7. Figure 1b shows TORAY-GA calculated ray trajectories and the approximate location of the X3 resonance. The RF beam was projected slightly toward the high field side of the resonance to benefit from absorption on the relativistically broadened resonance.

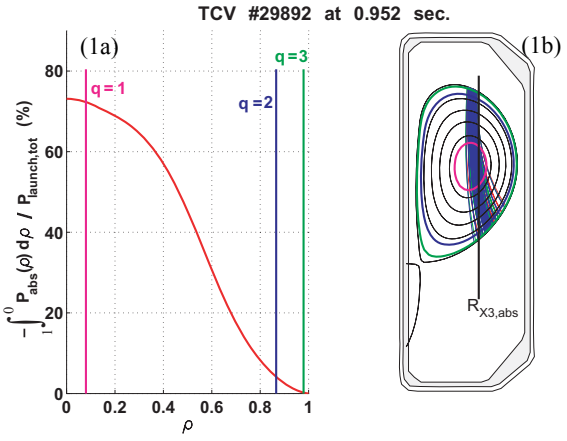

FIG 1: *(a) Beam integrated, incremental X3 absorption as a function of normalised radius. The absorption, and hence the heating, occur place between ρ ≈ 0.7 and ρ ≈ 0.1. (b) TORAY-GA calculated ray trajectories superimposed on the flux contours of the discharge and the approximate location of the X3 resonance shown by the black line.*

2.2 Quasi-stationary, ELM-free H-mode Plasma

Under heating conditions described above, the ELMy H-mode discharges frequently exhibited a transition from the ELMy H-mode to a quasi-stationary, ELM-free H-mode phase. This regime was characterised by elevated D_α light emission compared to the Type III ELMy H-mode, approximately constant line averaged electron density (n_{el}), constant W_{dia}, high β_{tor} and high τ_E. An example of this remarkable quasi-stationary ELM-free H-mode is shown in Figure 2.

This discharge entered a quasi-stationary ELM-free phase at 0.85sec that lasted, until 1.1sec; ≈ 10 confinement times. At this time the discharge entered a brief ELM-free H-mode period before entering a second quasi-stationary ELM-free H-mode phase that continued until 1.4sec.

The electron pressure profiles were very similar in the ohmic H-mode phase, the X3 heated ELMy H-mode phase and the quasi-stationary H-mode phase. During the quasi-stationary H-mode phase, measured β_{tor} was ≈ 2.5% (c.f. $\beta_{limit,ideal}$ ≈ 3.5%) and the confinement time for these discharges was ≈ 30msec, $H_{IPB98(y,2)}$ ≈ 1.4, at full heating power. Values of $H_{IPB98(y,2)}$ ≈ 1.7 have been achieved.

In the ohmic phase the density peaking factor, $n_{e,o}/n_{el}$, was ≈ 1.68 while in the ELM-free quasi-stationary phase it was reduced very slightly to ≈ 1.55. Numerical simulation, using KN1D code [14] indicated that edge fuelling played no role in maintaining the density peaking in these discharges. The low loop voltage in these discharges also suggested that the Ware pinch cannot be invoked to explain the density peaking. Some anomalous pinch must be at work [15, 16]. Measurements of soft X-ray emission revealed no sign of impurity accumulation during the quasi-stationary ELM-free phase; Z_{eff} ≈ 2.5 in the ohmic phase and increased to ≈ 3 in the X3 phase. These measurements are significant for they show that in reactor relevant conditions (β_N ≈ 2 with massive electron heating) there is an anomalous particle pinch that causes the density profile to be peaked. In a reactor this density peaking could enhance fusion reactivity and/or destabilise pressure gradient driven MHD instability.

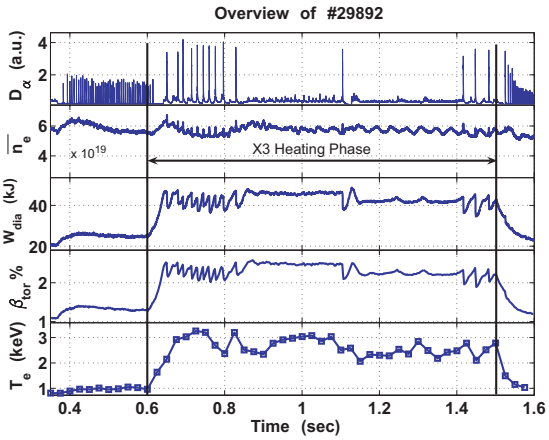

FIGe 2: Overview of TCV shot 29892. From top to bottom, the D_α light, line averaged density ($n_{el} \approx$ constant at $7.0\times10^{19}m^{-3}$), the stored energy, β_{tor} and electron temperature. This discharge was an ELMy H-mode target heated with ≈ 1.4MW of total heating power in the period 0.6sec until 1.4sec.

See Weisen et al [20].

The quasi-stationary ELM-free H-mode described here is reminiscent of both the quasi-stationary ELM-free H-mode observed on DIII-D [17] and the EDA H-mode on ALCATOR C-MOD [18]. However, there are some fundamental differences. On DIII-D neutral beam injection and cryo-pumping are required. The quasi-stationary ELM-free H-mode on TCV has no direct ion heating, no active fuelling and no cryo-pumping. The DIII-D quiescent H-mode is accompanied by an Edge Harmonic Oscillation (EHO) that is believed to control the plasma density during DIII-D quiescent H-mode. A similar edge oscillatory mode has not been observed on TCV. On ALCATOR C-MOD the EDA H-mode exhibits high energy confinement and high levels of recycling light as does the TCV quasi-stationary ELM-free H-mode. However, the EDA H-mode is generally obtained at $q_{95} > 3.7$ while on TCV the quasi-stationary ELM-free H-mode is obtained at $q_{95} \approx 2.5$. Also, the EDA H-mode is accompanied by broad-band and coherent fluctuations in the edge density that are believed moderate the core plasma density. Similar fluctuations have yet to be observed on TCV.

The quasi-stationary ELM-free phase of TCV H-mode discharges did exhibit some core MHD. They were typically dominated either by m/n = 1/1 modes associated with sawteeth (present throughout the discharges) or by m/n = 4/3 tearing modes that were associated with reduced energy confinement compared to the m/n = 1/1 dominated phases. The fluctuations observed on the D_α light during the quasi-stationary ELMy H-mode phase are not ELMs. In fact they are strongly correlated with the core MHD.

During the quiescent H-mode phase it was possible to measure the carbon ion toroidal rotation, $v_{tor,C}$, and carbon ion temperature profiles, T_C. These measurements were made using TCV Charge Exchange Recombination Spectroscopy (CXRS) diagnostic [19]. Due to the line of sight used by the CXRS system it was not possible to obtain measurements of T_C and $v_{tor,C}$ at $\rho < 0.6$.

Figure 3 shows the temporal evolution of the D_α recycling light, the T_C and $v_{tor,C}$, both at $\rho \approx 0.6$, for shot 29475. The X3 heating phase lasted from 0.6sec to 1.4sec. For the first time significant ion heating has been measured on TCV: it is interesting to note that $T_e \approx 3T_i$

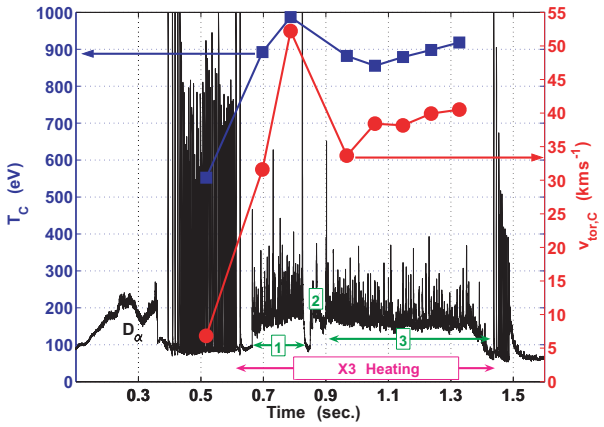

FIG 3: D_α light with the temporal evolution of the carbon ion temperature and carbon ion toroidal rotation velocity at $\rho \approx 0.6$ for shot number 29475. Shown also are the X3 heating phase (pink) and the three quasi-stationary H-mode phases (green) labelled 1, 2 and 3.

satisfying the criteria for maximum energy transfer from electrons to ions. At mid-radius the ion temperature increased from ≈ 500eV to ≈ 1keV. At the same time the carbon ion toroidal rotation speed was measured to increase significantly; this is despite the fact that the X3 heating produces no net momentum. In this discharge there were three ELM-free phases. The first (1), in the period 0.68sec to 0.83sec, was dominated by a m/n=1/1 mode while the second (2), in the period 0.84sec to 0.9sec was dominated by an m/n=4/3 mode. During this period there was significant degradation of the plasma performance and both the T_C and the $v_{tor,C}$ fell. In the third (3) quasi-stationary ELM free phase in the period 0.9sec to 1.37sec the discharge was again dominated by m/n = 1/1 modes and both the T_C and $v_{tor,C}$ partially recovered.

By optimising X3 coupling to ELMy H-mode plasma it has been possible to achieve reactor relevant plasma conditions on TCV. We are able to achieve $\beta_N \approx 2$ and significantly heat ions through the electron → ion collision channel. Under these conditions it has been shown that, contrary to predictions [22], the electron density profile remains significantly peaked pointing to an anomalous particle pinch. At the same time the electron density remains constant while the energy content nearly doubles. For reasons yet to be explained all this is achieved while diminishing first wall erosion by removing the ELMs and maintaining moderate particle confinement but good energy confinement ($H_{IPB98(y,2)} \approx 1.7$).

3. Suprathermal Electron Dynamics

In the very high power density conditions of X2 ECCD experiments in TCV, the dynamics of the high-energy electrons accelerated by the EC waves is unusually complex, as rf diffusion, collisional slowing-down and pitch-angle scattering in velocity space and cross-field transport in physical space all operate on comparable characteristic time scales [3]. In particular, radial transport has the effect of regulating the quasi-linear enhancement of ECCD efficiency and of broadening the driven current profile. The fundamental role played by suprathermal electrons in some of the key scenarios developed and explored in TCV has motivated a series of dedicated studies of the energetic electron dynamics under controlled conditions.

These studies employed periodic, low-duty-cycle bursts of ECRH (X2 ECCD or X3) in conjunction with high-field-side ECE measurements, which were coherently averaged over a

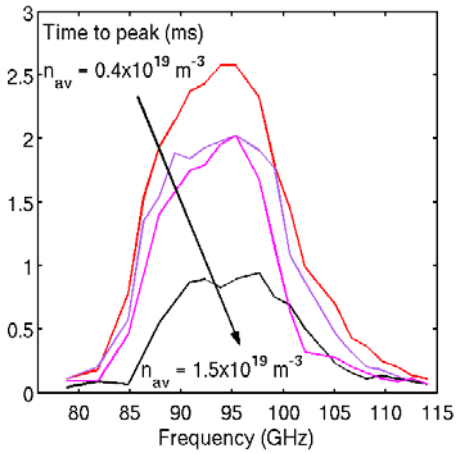

FIG 4: time-to-peak of HFS ECE from pulsed ECCD, as a function of frequency and line-averaged plasma density.

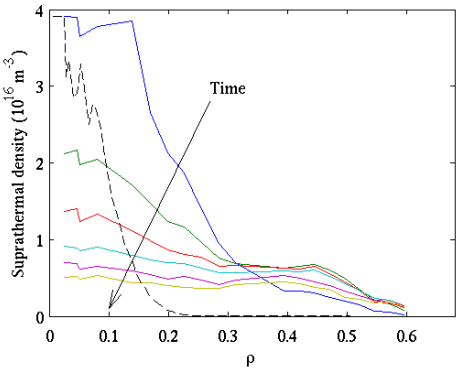

FIG 5: reconstructed suprathermal density profiles at times 0, 0.1, 0.2, 0.3, 0.4 and 0.5 ms after the ECCD turn-off; the time order is as indicated by the arrow. The dashed curve is the power deposition profile calculated by ray tracing, in arbitrary units. Average injected power 40 kW, plasma current 230 kA, line-averaged density 1.5x10^{19} m^{-3}.

stationary period comprising several tens of pulses [21]. The low average injected power ensured that the plasma was not significantly perturbed. The aim of this work was to follow the signal dynamics after power shut-off and identify the characteristic relaxation times and the full dynamical characteristics of the system.

The study was articulated in a series of systematic scans of plasma and ECRH parameters. The time-to-peak is an appropriate simple parameter to illustrate the dynamics, as it depends on both the characteristic transport time and the slowing-down time. The effect of radial transport was clearly seen in the time-to-peak plotted as a function of frequency (Fig. 4), for a case with centrally applied ECCD pulses and the ECE horizontal sightline lying on the plasma mid-plane. The rise at low frequency corresponded to X2 emission from locations increasingly off-axis on the HFS, whereas the rollover at high frequency was attributed to X3 emission from the LFS moving towards the center. The strong reduction of the time-to-peak with increasing density reflects primarily the corresponding reduction in the slowing-down time [21].

Resolving both the energy and the emission location in HFS ECE measurements is impossible. However, quantitative insight was obtained by adopting a simple bi-Maxwellian approximation for the electron distribution function. Employing the further assumption, verifiable *a posteriori*, that the relatively tenuous suprathermal component was optically thin, the suprathermal density profile was recovered from the ECE data [22]. As shown in Fig. 5, the spatial broadening caused by radial transport, as well as the overall temporal decay of the population caused by collisional momentum destruction, were clearly visualized through this technique. A simple diffusive model was applied to this case, allowing a representative diffusivity and decay time to be derived by a fit to the data, as shown in Fig. 6. The resulting diffusivity (12.6 m^2) was well above the typical values cited in the literature; this result must be seen as merely illustrative of the transport process at play, owing to the simplicity of the model. More extensive semi-analytical or Fokker-Planck modelling will be required to further constrain the system dynamics. It is worth noting that in a study of suprathermal electrons accelerated (to 10 – 15 keV) by the electric fields generated by sawtooth crashes in TCV, the radial diffusivity was been estimated to on the order of 25m^{2}s^{-1}[23].

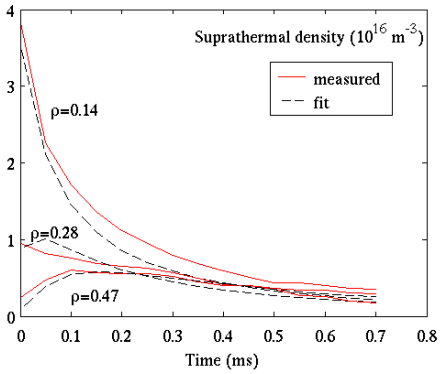

FIG 6: measured and fitted time traces of the suprathermal density at three different radial locations, for the case of Fig. 5. The fit is based on a cylindrical diffusive model with diffusivity D=12.6 m^2/s and decay time t=1.5 ms.

The suprathermal electron population generated by X2 ECCD is also believed to be responsible for the observed enhanced absorption of laterally-launched X3 waves with respect to calculations based on a Maxwellian population [4]. Recent work has demonstrated that a simplified ad-hoc electron distribution function model (in this case a combination of two truncated Maxwellians) can succeed in reproducing all the salient measurements, namely the power absorption, the ECE radiative temperature and the hard X-ray emissivity [23].

In another set of experiments the energetic electron dynamics were investigated by using X3 to couple to electrons in the hot electron tail of thermal plasma [5, 8] when the central plasma density was low ($< 2.5\times10^{19}m^{-3}$). The absorption of vertically launched X3 waves was measured and found to be larger than that predicted by TORAY-GA. The difference was attributed to the generation of a suprathermal population by the X3 wave itself, which in turn gave rise to enhanced absorption of the wave. This suprathermal population was clearly detected by a high field side second harmonic ECE radiometer. The radiative temperature was in excess of that measured by a Thomson scattering diagnostic. Also by sweeping the X3 beam from larger to smaller major radii it was observed that a signal related to the thermal energy, soft X-ray emission, peaked at an earlier time than the characteristic ECE suprathermal signal. At the time the latter reached its maximum, most of the beam propagation occurred well away from the nominal cold X3 resonance region indicating that absorption was occurring on a high energy electron tail. See Figure 7b.

The energy selectivity implied by the nearly one-to-one correspondence of major radius and energy opens the possibility of a particularly surgical form of distribution function engineering in velocity space. The spatial localization of the absorption is poor, however.

4. Conclusions

The extensive ECRH/ECCD capability on TCV has allowed advances in direct plasma heating at elevated density in H-mode plasma and the study of fast electron dynamics.

Electron heating of H-mode discharges has lead to a regime of quasi-stationary ELM-free H-mode with $H_{IPB98}(y,2) < 1.7$. Ion heating, through the electron – ion collision channel, has been demonstrated and in these discharges the electron density profiles remain peaked indicating of the presence of an anomalous particle pinch.

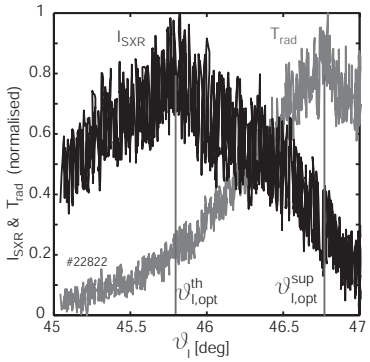

FIG 7b: SXR and T_r as a function of θ_L. It is seen that the optimal coupling to the bulk plasma and the fast-electron tail occur at differing angles indicating the presence of a fast-electron tail generated by the X3 wave itself.

Fast electron dynamics studies have concentrated on their transport and their effect on the absorption of X3 radiation. Fast electron diffusivity has been measured to be high but further modelling work is required to verify this. In accord with theory, enhanced X3 absorption has been measured in the presence of a fast-electron population.

Acknowledgements

This work was partly supported by the Fonds National Suisse pour la Recherche Scientifique.

References

[1] T.P. GOODMAN et al, Nucl. Fusion **36** B277
[2] P. BLANCHARD et al, Plasma Phys. Control. Fusion **44**, 2231 (2002).
[3] S. CODA et al, Nucl. Fusion **43**, 1361 (2003).
[4] S. ALBERTI et al., Nucl. Fusion **42**, 42 (2002).
[5] G. ARNOUX et al, Plasma Phys. Control. Fusion **47**, 295 (2005).
[6] S. ALBERTI et al, Nucl. Fusion **45**, 1224 (2005).
[7] I. KLIMANOV et al, Rev. Sci. Instrum. **76**, 093504 (2005).
[8] G. ARNOUX Ph.D. Thesis 3401, Ecole Polytechnique Fédérale de Lausanne (2005).
[9] ITER Physics Expert Groups on Confinement and Modelling 1999 Nucl. Fusion **29(**12)
[10] S. CODA et al, Phys. Plasmas **12**, 056124 (2005).
[11] L. PORTE et al; Proc. 20th IAEA Conf. on Fusion and Energy, Lyon, France Oct. 2002
[12] A MANINI et al 2002 Plasma Phys. Control. Fusion **44**(2) 139-157
[13] K. MATSUDA 1989, IEEE Trans. Plasma Sci. 17 6
[14] B. LABOMBARD 2001, PSFC, MIT Report PSFC/RR-01-3
[15] A. ZABOLOTSKY et al 2006 Plasma Phys. Control. Fusion **45** 745-746
[16] H. WEISEN et al 2006 Plasma Phys. Control Fusion **48** A457-466
[17] K. BURRELL et al 2002 Plasma Phys. Control. Fusion **44** A253-A263
[18] M. GREENWALD, R BOIVIN et al 2000 Plasma Phys. Control. Fusion **42** A263-269
[19] A.SCARABOSIO et al 2006 Plasma Phys Control Fus **48** 663-683
[20] H. WEISEN et al; EX8-4; "Peaked Density Profiles in Low Collisionality H-modes in JET ASDEX Upgrade and TCV"; this conference
[21] S. CODA et al, Proc. 30th EPS Conf. on Control. Fusion and Plasma Phys. (St. Petersburg, 2003)
[22] S. CODA et al, to be published in Plasma Phys. Control. Fusion (2006).
[23] I. KLIMANOV, Ph.D. Thesis 3432, Ecole Polytechnique Fédérale de Lausanne (2005).